E-6618

NASA TECHNICAL MEMORANDUM

NASA TM X-67943

NASA TM X-67943

BACKWARD ELASTIC pd SCATTERING AT 316, 364, 470 AND 590 MeV

by J. C. Alder, W. Dollhopf, C. Lunke, C. F. Perdrisat, W. K. Roberts, P. Kitching, G. Moss, W. C. Olsen, and J. R. Priest
Lewis Research Center
Cleveland, Ohio

TECHNICAL PAPER proposed for presentation at
Southwest Section Meeting of the American Physical Society
Columbia, South Carolina, November 4-6, 1971

BACKWARD ELASTIC pd SCATTERING AT 316, 364, 470 AND 590 MeV

By J. C. Alder,+‡ W. Dollhopf,+ C. Lunke,+‡ C. F. Perdrisat,+
W. K. Roberts, P. Kitching,* G. Moss,* W. C. Olsen,*
and J. R. Priest**

Lewis Research Center
National Aeronautics and Space Administration
Cleveland, Ohio

ABSTRACT

We report preliminary results from a part of the data obtained at the NASA Space Radiation Effect Laboratory for the elastic scattering of protons by deuterons in the backward hemisphere, at a number of energies between 300 and 600 MeV.

INTRODUCTION

It has been known for some time that above 300 MeV, the backward elastic (pd) differential cross section was larger than one would expect on the bases of a single-nucleon exchange mechanism. There was a renewed interest in this problem when data at 1300 MeV[1], and 1000 MeV[2], and later 590 MeV[3] became available. A possible explanation of the anomalous backward scattering was proposed by Kerman and Kisslinger[4] in terms of an admixture of excited nucleon states in the ground state of the deuteron. It was found that if the probability for the ground state of the deuteron to be a normal nucleon and a (5/2, 1/2) nucleon isobar with invariant mass 1688 MeV, was 2 percent, the results of experiments of references 2 and 3 could be explained. The 1688 MeV isobar is the lowest nucleon excited state that can exist in the deuteron, unless both nucleons are excited. The different possible components of the deuteron ground state with isobars are discussed for example by Arenhövel, Danos, and Williams[5].

Along different lines, a model was proposed by Crougie and Wilkin[6] who argued that for laboratory energies around 600 MeV, triangular graphs with a neutron- and a pion-line connecting the observed states should be more important than the one-neutron exchange diagram.

+College of William and Mary, Williamsburg, Virginia.
‡Fellows of the Swiss Institute for Nuclear Research (S.I.N.) Zurich, Switzerland.
*University of Alberta, Edmonton, Alberta, Canada.
**Miami University, Oxford, Ohio.

A neutron-pion exchange graph is probably dominant in the process $pp \rightarrow d\pi^+$, which is known to have a resonant-like behavior with a maximum at 600 MeV. The resonant behavior in $d\pi^+$ final state is believed to be associated with the (3/2, 3/2) 1236 MeV resonance in the nucleon-pion system, which would enhance reactions in which the nucleon and pion exchanged have an invariant mass near that of the (3/2, 3/2) resonance. This situation occurs also in the pd system. Wilkin[7] calculated the (pd) elastic cross section near 180° with no free parameter and obtained excellent agreement with the data of reference 3.

In still another effort to understand (pd) scattering, Remler et al.[8] have been investigating the lower energy data in terms of single-nucleon exchange, single-scattering and multiple-scattering contributions. The data below 300 MeV is being used to determine a number of parameters to describe the third contribution. An extrapolation of these parameters to the energy region where other mechanisms may be important is expected to demonstrate the existence of new terms in the interaction.

The current strong interest in the pd system justified an investigation of the backward angular region for the elastic channel in the domain of energy available at SREL. About the time this experiment was started, we received the data obtained at Chicago by Booth et al.[9] at 415 MeV. Earlier experiments were at 340 MeV[10] and 660 MeV[11] but included few data points, each with relatively large uncertainty in the backward hemisphere.

DESCRIPTION OF THE EXPERIMENTAL SETUP

Figure 1 is a drawing of the experimental arrangement. The experiment was performed at 4 energies 590 MeV, 470 MeV, 364 MeV, and 316 MeV. Beams with energies lower than the normal 590 MeV beam were obtained by placing copper degraders in the upstream part of the transport system. Manipulation of the transport magnet system was necessary to obtain small beam spots on target and small beam divergence. Whereas the beam spot at the target position at normal energies was 1.8 cm by 2.5 cm (horizontal by vertical), it was not possible to maintain this size with degraded beam energies without adversely affecting the beam divergence. The beam spots on target at the reduced energies were 3.7 cm by 5.0 cm, 3.7 cm by 3.7 cm, and 4.0 cm by 4.0 cm at 470 MeV, 364 MeV, and 316 MeV, respectively.

The incident proton intensity was monitored by scattering protons into a 3-counter telescope from an auxilliary aluminum target 0.6 cm thick placed 6 meters downstream from the CD_2 target. The monitor target was 30 x 30 cm^2 and pictures were taken for each beam energy to insure that the spot size did not exceed the monitor target dimensions. The beam monitor was calibrated using the ^{12}C (p, pn) ^{11}C (Ref. 12) reaction on graphite targets. The number of activated nuclei was determined by counting the annihilation photons of the positrons emitted in the decay of ^{11}C in a calibrated geometry. A monitor calibration was made for each new beam energy but was not repeated every time the same energy

was set up, except for the 364 MeV beam. The two calibrations at this energy gave results different by two standard deviations (the standard deviation for each calibration is about 1.5 percent; the absolute uncertainty due to the probable error of the $^{12}C(p, pn)^{11}C$ cross section is 5 percent for each energy).

A single CD_2 target (hydrogen content less than 2 percent) 0.203 cm thick by 10 cm by 10 cm was used throughout the experiment. It was oriented so as to minimize multiple scattering of the backward scattered proton. Graphite targets 0.063 and 0.381 cm thick were used to measure the background contribution from the carbon in CD_2. The thin graphite target had 66 percent of the number of C-nuclei in the CD_2 target, and the thick one four times as many as in the CD_2 target.

The detection apparatus was a coincidence spectrometer (see Fig. 1). Deutrons scattered in the forward center of mass hemisphere were detected by three scintillators D_1, D_2, D_3 and three spark chambers. The three spark chambers provided three horizontal and two verticle coordinates. Counter D_1 was 45.8 cm from the target, 0.21 cm thick, and 7.6 cm high by 10.8 cm wide. Counter D_2 was 61 cm from the target, 0.21 cm thick, and 7.9 cm high by 11.1 cm wide. Counter D_3 was 600 cm from the target, 0.63 cm thick, and 25.4 cm high by 76.2 cm wide. The three spark chambers were located at 438.7 cm, 498.7 cm, and 589.3 cm from the target, and had sensitive regions larger than the solid angle defined by D_1, D_2, and D_3. Protons scattered in the backward cm hemisphere were detected in two scintillators P_1, P_2 and a set of three spark chambers. These spark chambers also provided three horizontal and two vertical coordinates. Detector P_1 was 51 cm from the target, 0.203 cm thick, and 12.7 cm wide by 5.7 cm high. Detector P_2 was 0.63 cm thick and 28 cm wide by 12.7 cm high. Detector P_2 was from 122 cm to 161 cm from the target during the experiment depending on the proton angle. The spark chambers had sensitive regions larger than the solid angle defined by P_1 and P_2.

A coincident event was defined as EVENT = $(D_1 \cdot D_2 \cdot D_3) \cdot (P_1 \cdot P_2)$. The master logic signal in EVENT was obtained from detector D_2. The time of flight of the particle detected in the deuteron arm was measured for each EVENT using EVENT as a start signal and the logic signal from detector D_3 as the stop signal for a time to amplitude converter. EVENT was also used to trigger a 5kV pulse generator which triggered a master spark gap. The master spark gap then triggered a number of spark gaps which provided the high voltage pulse for the various spark chambers. The spark planes were of the copper nylon mesh type (copper wire 0.0125 cm in diameter, spacing 0.05 cm) with magneto-striction readout.

The spark chamber readouts were interfaced with the Space Radiations Effects Laboratory on line computer via a commercial digitizing system. The time-of-flight information was also fed to the computer event by event using a 1024-channel analog-to-digital converter. All input to the computer was stored on magnetic tape along with a run number tag and

total monitor count and total EVENT count in that run for use in replay analysis. No discrimination based on time-of-flight was made during data taking, although later replay analysis included cuts framing the elastic deuteron peak observed in the time-of-flight spectrum.

On the basis of the known properties of the spark chambers and of the reaction kinematics it was expected that a sufficient criterion to reject inelastic events would be the angular correlation of the proton and deuteron. The spacial resolution of the chambers was good enough to provide a separation of the elastic events from all three-body final states from deuteron breakup, quasi-elastic reactions on the carbon in the CD_2 target and possible pion production final states as pdπ or pp$n\pi$. The analysis of the data confirmed the initial assumption.

In this report we will present only the data for proton laboratory angles larger than 95°; these were obtained with the deuteron detectors at 20, 12.5 and 10°. The angle of the proton detectors were chosen from kinematic tables. The horizontal proton detector aperture was 10, 12, and 13°, respectively, for the three deuteron angles above. The horizontal aperture of the deuteron counters was maintained constant at 7.3°. The aperture information given here refers to a point target. In the CM system for the pd final states, the forward horizontal acceptance was very nearly twice the backward acceptance. Therefore for every position of the forward leg we placed the proton telescope in two different positions in order to cover completely the forward acceptance. The experiment was planned with horizontal acceptances closely matched in the CM in order to minimize the number of spectrometer arm position changes. In the vertical direction however, the angular acceptance was always determined by counter P_2.

ANALYSIS OF THE DATA

As soon as the information associated with each event was placed in buffer regions of the computer memory, an attempt at geometrical reconstruction was made directly on-line, (allowing a check of the progress of the experiment). The data discussed here are the result of a later replay of the data tapes using essentially the same routines as during the run, although with slightly different cuts on some of the parameters.

Eight of the 10 spark plane coordinates were associated with four digitizer scalers each, the remaining two coordinates with two scalers. Although the spark multiplicity in any of the coordinates was always small (at the most 30 percent double sparks, 1 to 3 percent triples), the reconstruction routines were such that several spark combinations could be tried for a given event, until one satisfying all criteria was found. The fraction of events that required more than one attempt remained small (of the order of a few percent), in part because all of the cuts applied were wide. The effect of increasingly narrow cuts was

studied offline. For each acceptable event the following quantities were calculated and stored for display at the end of a run (a typical run contained 10 000 events): time-of-flight, distribution of the distance to the spark in the middle horizontal plane for the selected trajectory in the deuteron and proton detectors (a check of the plane spacial resolution), intersections of both trajectories with the target in horizontal and vertical directions, and the distance between intersections of the two trajectories in the vertical and horizontal directions (check of the correlated origin of the event), scattering angles in horizontal and vertical directions θ_p and θ_d, x_p and x_d, respectively, and coplanarity of the two trajectories calculated as the difference of the vertical angles projected in a plane perpendicular to the beam at the target.

To avoid the need of maintaining one of the CM solid angle larger than the other to minimize border- and resolution-effects, we classified the events in bins on the proton scattering angle θ_p and displayed for each of these bins the complete spectrum of the sum angles $(\theta_p + \theta_d)$. Each proton angle bin could then in first order be considered as a sub-experiment with complementary angle condition on the deuteron side satisfied, allowing for kinematics, multiple scattering of the particles in the different counters and target and intrinsic spacial resolution of the spark planes. Typically we divided the proton horizontal acceptance angle into 10 bins (varying in size from 1 to 1.2 to 1.3° for the three deuteron angles considered here), and examined also the content of two more bins on either side of the acceptance angle. By visual inspection we found that when the angles of the two detectors had been correctly matched, eight bins could be used without correction for finite resolution, beam size or multiple scattering. For each one of these proton bins the correlation angle spectrum in $(\theta_p + \theta_d)$ had typically a sharp peak, usually 2° FWHM, sitting on a wider background due to weakly correlated or uncorrelated events. Data taken with a graphite target never showed any peak, with the available domain of $(\theta_p + \theta_d)$ merely filled uniformly. The background from the graphite target was measured for every angle and for every energy. The subtraction of the C contribution was made taking into account the numbers of carbon nuclei in the CD_2 and graphite targets and the number of incident protons in the CD_2 and graphite runs. Checks of the C substraction were made both on the time-of-flight and angular correlation spectra. When no time-of-flight cuts were applied, the continuum under the elastic peak in the correlation spectra was always more important; but we obtained the same cross sections within statistical error, whether we applied cuts on the time-of-flight or not. We also verified that when the C subtraction did not remove the background in the correlation spectra completely, an artificial increase of the C spectrum compatible with the time-of-flight spectra would not affect the result by more than one statistical error. All the data presented here were submitted to these two tests.

The time-of-flight spectra for the CD_2 and graphite target were systematically different. Whereas at the two highest energies, the only difference noticed was in the position of the deuteron peaks, at the lower energies shape differences were also noticeable. At 590 MeV the "deuteron" peak (that we interpret as originating in quasi-elastic C(p, pd) reactions) was late for the graphite target by about 0.20 ns/m relative to the elastic deuteron peak characteristic of the CD_2 data, at 470 MeV this delay increased to about 0.25 ns/m. At these two energies the widths of the graphite "deuteron" peak was only slightly larger than that of the elastic deuteron peak (in agreement with what is known of the Fermi momentum distribution of deuterons in carbon as observed by Sutter et al.[12]); the deuteron peak from the graphite target was however riding on some continuum which we have not yet identified. At the two lower energies the graphite-target "deuteron" peak was also late (0.4 ns/m at 364 MeV, 0.9 ns/m at 316 MeV) but also significantly wider than the elastic peak (up to twice at the lower energy). It is likely that at least part of this widening is the result of the smearing from internal momentum of the deuterons in carbon, but this point has not been checked quantitatively yet.

The number of graphite-target events falling within the time-of-flight window applied on the CD_2 data shows a systematic dependance both on the incident energy and on the proton scattering angle θ_p. Whereas at 590 MeV a comparison of the time-of-flight spectra from the CD_2 and graphite targets indicates that we subtract the background precisely, it is possible that we have not subtracted enough background at the lower energies (the difference spectrum shows a shoulder remaining on the side of slow particles). However, if we assume that the difference spectrum should have no shoulder and multiply the graphite spectrum by an appropriate factor to make the shoulder disappear, we find cross sections that differ from those quoted below by less than the statistical error. The maximum ad-hoc factor by which the C background should be multiplied is about 2.5.

The background subtraction for the CD_2 data was maximum at the highest energy and the smallest value of $\overline{\theta}_p = 98°$: 37.7 percent. ($\overline{\theta}_p$ is the laboratory angle of the proton detector centerline.) The minimum correction applied to the CD_2 was at the lowest energy and for the largest value of $\overline{\theta}_p = 144°$: 1.5 percent. One might be tempted to interpret these fractions in terms of probabilities for a deuteron to exist in carbon. However this is permissible only if the experimental solid angles were large enough to accept all events, regardless of the amount of decorrelation resulting from the Fermi momentum of deuterons in carbon nuclei. It appears that we did not have a large enough solid angle for that. It is understandable that as the energy of the incident particle decreases, the number of "deuterons" in the graphite target background should do likewise, as for smaller momenta of the outgoing particles the decorrelation from Fermi motion becomes more severe. Also, for increasing proton angles the proton momentum gets smaller and the Fermi momentum increasingly throws the protons out of the solid angle.

In short we understand the general features of the energy- and angular-dependance of the graphite-target data but there remains an uncertainty as to the exact amount of background to be subtracted. Thus it appears safe to assume that there may be a systematic error from the smallest to the largest angle at any given energy of about 5 percent due to background subtraction.

Calculation of the Cross Section

The cross section for each proton bin of width $\Delta\theta_p$ around θ_p was calculated from

$$\frac{d}{d\Omega_p} = \frac{N(\theta_p) \times \cos\theta_{tgt}}{\Delta\Omega_p \times n \times I \times E_{sc}} \; ; \; \Delta\Omega_p = \frac{\Delta\theta_p}{57.3} \times \frac{\text{height of } P_2}{\text{distance to } P_2}$$

where $N(\theta_p) = (N_{CD_2}(\theta_p) - N_C(\theta_p))$ is the number of elastic deuteron events (after proper background subtraction) that where reconstructed; θ_{tgt} is the angle of the target plane with the normal to the beam. n is the number of deuterium nuclei within the CD_2 target and I = (Monitor) x (Calibration) is the number of incident protons in a run. E_{sc} is the overall spark plane efficiency, and includes both sparking and reconstruction efficiencies. The definition and estimate of the efficiency E_{sc} present some inherent difficulty. We evaluated E_{sc} as the ratio of the total number of reconstructed events in a run that satisfy a number of conditions described below (and which did not include time-of-flight), to the number of "true" triggers (EVENT), defined as the difference between real triggers and chance coincidences $\overline{EVENT} = (D_1 \cdot D_2 \cdot D_3)$ 56 ns $(P_1 \cdot P_2)$. Implied in the definition of "true" triggers is the assumption that chance coincidence $\overline{EVENT}$ were not reconstructed; we verified experimentally that $\overline{EVENT}$ triggers had less than 5 percent probability to be reconstructed.

The condition imposed on reconstruction were of three types. First each group of horizontal and vertical planes on the deuteron and proton side (for a total of four groups) were scanned for tracks in the order HD, HP, VD, VP (for horizontal deuteron, horizontal proton, and so on). A track was defined as two sparks through which a straight line projected to the target would intercept the target within prescribed distances from the target center (either vertically or horizontally). Or, for the horizontal coordinates, where three planes were available, it was first checked whether a straight line through the first and last plane's sparks would intercept the middle plane within chosen distance from a spark in that plane; then the target intersection test was made. Second, the events having passed the first test where checked for correlation in origin: the distances between the two intercepts from the selected tracks on each side had to be within prescribed values. Fail-

ure at any of the previously mentioned checks resulted in further scanning for other sparks which would give satisfactory two-correlated-track events. The fraction of true events (defined previously) that would satisfy the two tests before mentioned was usually between 70 and 80 percent; lower efficiencies were observed when one of the spark planes showed obvious poor sparking efficiency (usually due to insufficient gas flushing) or when the fraction of accidental coincidence in EVENT was large due to too high a beam intensity or bad stochastic properties of the beam. The fraction of accidental triggers was kept under 10 percent for most CD_2 runs, but was usually larger for graphite targets.

The third check was related to the coplanarity of the events: two-body final states must be contained in one plane. The efficiencies calculated for coplanarity cuts of $\pm 5^\circ$ (twice the observed FWHM) seem to be too low; the cross sections we obtain this way are systematically larger than those without coplanarity requirement. To check whether this discrepancy was related to the way the spark chamber efficiency was evaluated, we redefined an efficiency E'_{sc} as the ratio of the number of reconstructed events with a time-of-flight corresponding to a deuteron (± 0.55 ns/m from the elastic peak) to the number of "true" triggers within the same time-of-flight interval. It was found that $E_{sc} \sim E'_{sc}$ to within 1 percent.

Figure 2a shows a typical time-of-flight spectrum for CD_2 and graphite targets. Figure 2b shows the corresponding correlation spectrum ($\theta_p + \theta_d$). Figure 2c shows the coplanarity spectrum for all proton angles with $\theta_p = 10^\circ$. The coplanarity angle is defined as $x = (x_p/\sin\theta_p) + (x_d/\sin\theta_d)$, where x_p and x_d are the angles relative to the horizontal plane of the proton and deuteron trajectory, respectively.

The relatively wide spectrum observed for the coplanarity angle is not as bad as it might seem if one realizes that through projection of the vertical scattering angles x_p and x_d on the plane perpendicular to the beam at the target, we are multiplying these angles and therefore their error by typical factors of 4.6 on the deuteron side, 1.5 on the proton side (these numbers are valid for 12.5° deuterons and 130° protons). Furthermore, because we had only two vertical coordinates in each telescope, the rejection of spurious sparks could not be as efficient as for horizontal projections. We feel that the results obtained with checks one and two above are better than those for which check three has been added. The cross sections presented in the next part are obtained without coplanarity requirement (checks one and two only).

RESULTS AND DISCUSSION

The cross sections were first calculated for every proton angle bin as described in the previous part. A weighted average was then obtained taking two bins at a time. The results are given in tables I to IV. The data in these tables are differential cross sections averaged over a 2° interval for $\theta_{pcm} \leq 111.5^\circ$ over 2.4° for $118.4^\circ \leq \theta_{pcm} \leq 136.6^\circ$ and 2.6° for $\theta_{pcm} \geq 137.2^\circ$ (the θ_{pcm} values are for 590 MeV they vary slightly as a function of energy).

Figure 3 shows $\log(d\sigma/d\Omega)_{pcm}$ as a function of $\cos(\theta_{pcm})$ at 590 MeV, 470 MeV, 364 MeV, and 316 MeV. The errors in tables I to IV and figure 3 are statistical only. As discussed in the preceeding parts, we estimate possible systematic errors as follows: (a) at a given energy, over the angular range presented, ± 5 percent; (b) from one energy to any other, ± 8 percent; the latter number includes 5 percent for the $^{12}C(p, pn)^{11}C$ cross section uncertainty, 1.5 percent for statistics in the monitor calibration, and 5 percent for uncertainties on beam characteristics reproducibility (beam spot size, position at the monitor target, and divergence).

The data as presented here is averaged over a proton angle interval which corresponds to the angular resolution on the correlation angle $(\theta_p + \theta_d)$, given the proton bin used in the data analysis. The precision of angle measurements is estimated as (a) $\pm 0.1^\circ$ on the reproducibility of θ_p, (b) $\pm 0.01^\circ$ on the reproducibility of θ_d, and (c) ± 0.025 for the absolute position of the deuteron counter relative to the beam line (0.3 cm at 600 cm).

In figure 3a we show also the results of out 1969 experiment at 590 MeV (Ref. 3). The new cross sections are systematically 20 percent lower and we have presently no explanation for this discrepancy.

A comparison of the data plotted in figure 3 leads to the following remarks. In the half-logarithmic representation chosen the CM cross section is very nearly linearized. It is not obvious that a $\cos\theta_{pcm}$ display is the most meaningful one, beyond the near linearization obtained. We notice that if we call $-t$ the four-momentum transfer squared, then

$$\cos\theta_{pcm} = 1 + \left(\frac{t}{2p_{cm}^2}\right)$$

where p_{cm} is the CM momentum; therefore the $\cos\theta_{pcm}$ representation shows in fact directly the $-t$ dependance of the CM cross section. On the other hand if q is the Fermi momentum of the neutron in the single-nucleon exchange process, then

$$\cos\theta_{pcm} = \left(\frac{q^2}{p_{cm}^2}\right) - \frac{5}{4}$$

therefore the $\cos\theta_{cm}$ representation is not meaningful if the process is dominated by single-neutron exchange. A q-representation would be better.

It is obvious from Fig. 3 that for any given value of θ_{pcm} or $-t$ displayed, the CM cross section is nearly the same (to within ±10 percent) at the three higher energies. By extrapolating visually to $\cos\theta_{pcm} = -1.0$ straight line fits in Fig. 3 we find values of $(d\sigma/d\Omega)_{cm}$ 180° shown as a function of the proton laboratory energy in Fig. 4. Data from other experiments have been included (see references in INTRODUCTION). We have dropped the ancient results of Refs. 10 and 11. The energy region between 100 MeV and 300 MeV shows a fast drop of the CM cross section and is well understood (Ref. 8) in terms of single-neutron exchange and multiple scattering; the cross section is directly related to $|\phi(\Delta)|^2$, the momentum space single-particle deuteron wave function squared. $\Delta = |\vec{\Delta}|$ is defined as in Ref. 4:

$$\vec{\Delta} = \frac{\vec{d}_{out}}{2} - \vec{p}_{in}$$

where $\vec{d}$ and $\vec{p}$ are CM momenta. Around 300 MeV we observe a definite flattening of the 180° CM cross section. It appears also likely that the cross section will start dropping again just above 600 MeV; the data points at 1000 and 1300 MeV show a fast drop indeed.

At this point we like to interpret Fig. 5 as a clear indication of either another reaction mechanism beside single-neutron exchange and multiple scattering, or another component in the deuteron ground state wave function beside the known S and D states. What is now needed is a detailed theoretical interpretation of the data in the energy range 300 to 1300 MeV.

REFERENCES

1. E. Coleman, R. M. Heinz, O. E. Overseth and D. E. Pellet, Phys. Rev. 164, 1655 (1967).

2. G. W. Bennett, J. L. Friedes, H. Palevsky, R. J. Sutter, G. J. Igo, W. D. Simpson, G. C. Phillips, R. L. Stearns and D. M. Corley, Phys. Rev. Letters 19, 387 (1967).

3. J. S. Vincent, W. K. Roberts, E. T. Boschitz, L. S. Kisslinger, K. Gotow, P. C. Gugelot, C. F. Perdrisat, L. W. Swanson and J. R. Priest, Phys. Rev. Letters 24, 236 (1970).

4. A. K. Kerman and L. S. Kisslinger, Phys. Rev. 180, 1483 (1969).

5. H. Arenhovel, M. Danos and H. T. Williams, Nucl. Phys. A162, 12 (1971).

6. N. S. Craigie and C. Wilkin, Nucl. Phys. B14, 477 (1969).

7. C. Wilkin, private communication, Nov. 1969.

8. E. A. Remler and R. A. Miller, private communication, Spring 1971.

9. N. E. Booth, C. Dolnick, R. J. Esterling, J. Parry, J. Scheid and D. Sherden, "Proton Deuteron Elastic Scattering at 1 GEV/C," Univ. Chicago, Enrico Fermi Inst. Preprint (1971).

10. O. Chamberlain and D. D. Clark, Phys. Rev. 102, 473 (1956).

11. G. A. Leksin, Soviet Phys. - JETP 5, 371 (1957).

12. J. B. Cumming, J. Hudis, A. M. Poskanzer and S. Kaufman, Phys. Rev. 128, 2392 (1962).

13. K. Kuroda, A. Michalowicz and M. Poulet, Nucl. Phys. 88, 33 (1966).

TABLE I. - p-D DIFFERENTIAL CROSS SECTION AT 590 MeV

Proton laboratory scattering angle $\theta_{p,lab}$, deg	Laboratory differential Cross section and error $\left(\frac{d\sigma}{d\Omega}\right)_{lab} \pm \Delta\left(\frac{d\sigma}{d\Omega}\right)_{lab}$ μb/sr	Proton center-of-mass scattering angle θ_{pcm}, deg	$\cos\theta_{pcm}$	Center-of-mass differential cross section and error $\left(\frac{d\sigma}{d\Omega}\right)_{cm} \pm \Delta\left(\frac{d\sigma}{d\Omega}\right)_{cm}$ μb/sr	Momentum transfer squared $-t$ $(GeV/c)^2$
95.5	16.2 ± 1.4	130.9	0.655	24.6 ± 2.2	1.67
97.5	16.9 ± 1.4	132.6	.677	26.7 ± 2.2	1.70
99.5	18.9 ± 1.4	134.3	.698	31.3 ± 2.3	1.72
101.5	20.0 ± 1.4	136.0	.719	34.9 ± 2.5	1.74
105.5	23.3 ± 1.3	139.1	.756	44.3 ± 2.5	1.78
107.5	24.4 ± 1.3	140.7	.774	48.5 ± 2.6	1.79
109.5	24.4 ± 1.2	142.2	.790	50.0 ± 2.5	1.81
111.5	28.5 ± 1.3	143.6	.805	62.1 ± 2.8	1.83
118.4	31.8 ± 1.0	148.4	.852	81.3 ± 2.6	1.87
120.8	33.6 ± 1.0	150.0	.866	90.1 ± 2.7	1.89
123.2	37.0 ± 1.0	151.5	.877	104.0 ± 3.0	1.90
125.6	36.9 ± 1.0	153.0	.891	108.0 ± 2.9	1.91
130.5	39.4 ± 1.6	155.9	.913	125.0 ± 5.0	1.93
132.5	37.6 ± 1.6	157.1	.921	124.0 ± 5.0	1.94
134.6	39.8 ± 1.6	158.2	.929	136.0 ± 6.0	1.95
136.6	39.7 ± 1.6	159.3	.935	141.0 ± 6.0	1.95
137.2	39.6 ± 1.5	159.7	.938	140.0 ± 5.0	1.96
139.8	41.8 ± 1.5	161.1	.946	155.0 ± 6.0	1.97
142.4	44.0 ± 1.5	162.4	.953	170.0 ± 6.0	1.97
145.0	45.2 ± 1.5	163.8	.960	182.0 ± 6.0	1.98

TABLE II. - p-D DIFFERENTIAL CROSS SECTION AT 470 MeV

Proton laboratory scattering angle $\theta_{p,lab}$, deg	Laboratory differential cross section and error $\left(\frac{d\sigma}{d\Omega}\right)_{lab} \pm \Delta\left(\frac{d\sigma}{d\Omega}\right)_{lab}$ μb/sr	Proton center-of-mass scattering angle θ_{pcm}, deg	cos θ_{pcm}	Center-of-mass differential cross section and error $\left(\frac{d\sigma}{d\Omega}\right)_{cm} \pm \Delta\left(\frac{d\sigma}{d\Omega}\right)_{cm}$ μb/sr	Momentum transfer squared $-t$ $(GeV/c)^2$
97.5	21.6 ± 0.9	131.7	0.665	32.5 ± 1.3	1.33
99.5	23.5 ± 0.9	133.4	.687	37.2 ± 1.4	1.35
102	23.4 ± 0.7	135.5	.713	39.2 ± 0.8	1.37
105.5	28.4 ± 0.9	138.3	.747	51.8 ± 1.5	1.40
107.5	28.5 ± 0.9	139.9	.765	54.4 ± 1.6	1.42
109.5	31.6 ± 0.9	141.4	.781	62.1 ± 1.7	1.43
112	33.6 ± 0.7	143.2	.801	70.7 ± 1.5	1.44
118.4	39.7 ± 1.1	147.7	.845	95.9 ± 2.6	1.48
120.8	42.1 ± 1.1	149.4	.861	107.0 ± 3.0	1.49
123.2	44.5 ± 1.1	150.9	.874	119.0 ± 3.0	1.50
125.6	44.6 ± 1.1	152.4	.886	124.0 ± 3.0	1.51
129.9	46.1 ± 1.3	155.0	.906	135.0 ± 4.0	1.53
132.3	47.1 ± 1.3	156.4	.916	146.0 ± 4.0	1.54
134.7	50.6 ± 1.3	157.8	.926	163.0 ± 4.0	1.54
137.1	51.4 ± 1.3	159.2	.935	172.0 ± 4.0	1.55
139.7	44.5 ± 1.0	160.6	.943	156.0 ± 4.0	1.56
142.3	45.8 ± 1.0	162.0	.951	167.0 ± 4.0	1.56
144.9	45.6 ± 1.0	163.4	.958	173.0 ± 4.0	1.57

TABLE III. - P-D DIFFERENTIAL CROSS SECTION AT 365 MeV

Proton laboratory scattering angle $\theta_{p,lab}$, deg	laboratory differential cross section and error $\left(\frac{d\sigma}{d\Omega}\right)_{lab} \pm \Delta\left(\frac{d\sigma}{d\Omega}\right)_{lab}$ μb/sr	Proton center-of-mass scattering angle θ_{pcm}, deg	$\cos\theta_{pcm}$	Center-of-mass differential cross section and error $\left(\frac{d\sigma}{d\Omega}\right)_{cm} \pm \Delta\left(\frac{d\sigma}{d\Omega}\right)_{cm}$ μb/sr	Momentum transfer squared $-t$ $(GeV/c)^2$
99.5	23.9 ± 0.6	132.5	0.676	37.3 ± 0.9	1.03
101.5	27.2 ± 0.7	134.2	.697	43.7 ± 1.1	1.05
104.5	31.3 ± 0.8	136.7	.728	55.6 ± 1.5	1.07
106.5	34.0 ± 0.9	138.3	.747	63.3 ± 1.6	1.08
108.5	32.7 ± 0.9	139.9	.765	63.4 ± 1.7	1.09
110.5	32.7 ± 0.9	141.4	.782	66.1 ± 1.8	1.10
112.5	33.9 ± 0.9	142.9	.798	71.1 ± 1.9	1.11
121.5	37.8 ± 0.9	149.2	.859	95.4 ± 2.3	1.15
124.5	39.3 ± 0.8	151.1	.876	105.0 ± 1.0	1.16
131.8	43.0 ± 2.1	155.7	.911	131.0 ± 4.0	1.18
134.2	47.4 ± 2.2	157.1	.921	150.0 ± 4.0	1.19
137.2	43.6 ± 1.9	158.8	.932	144.0 ± 3.0	1.19
141.4	46.7 ± 0.9	161.1	.946	164.0 ± 3.0	1.20
144.0	47.2 ± 0.9	162.5	.954	172.0 ± 3.0	1.21
146.6	44.4 ± 0.9	163.9	.961	168.0 ± 3.0	1.21

TABLE IV. - p-D DIFFERENTIAL CROSS SECTION AT 316 MeV

Proton laboratory scattering angle $\theta_{p,lab}$, deg	Laboratory differential cross section and error $\left(\frac{d\sigma}{d\Omega}\right)_{lab} \pm \Delta\left(\frac{d\sigma}{d\Omega}\right)_{lab}$ μb/sr	Proton center-of-mass scattering angle θ_{pcm}, deg	$\cos \theta_{pcm}$	Center-of-mass differential cross section and error $\left(\frac{d\sigma}{d\Omega}\right)_{cm} \pm \Delta\left(\frac{d\sigma}{d\Omega}\right)_{cm}$ μb/sr	Momentum transfer squared $-t$ $(GeV/c)^2$
109.0	40.4 ± 0.7	139.9	0.765	74.4 ± 1.5	0.939
111.0	39.9 ± 0.7	141.4	.782	79.7 ± 1.5	.946
113.5	38.5 ± 0.7	143.3	.801	81.3 ± 1.6	.958
122.3	34.8 ± 0.8	149.4	.861	87.0 ± 1.9	.990
124.7	38.6 ± 0.8	151.0	.875	100.0 ± 2.0	.997
127.1	40.7 ± 0.8	152.5	.887	111.0 ± 2.0	1.004
130.2	38.1 ± 0.7	154.4	.902	111.0 ± 2.0	1.01
132.6	38.6 ± 0.8	155.9	.913	117.0 ± 2.0	1.02
135.0	37.8 ± 0.8	157.3	.923	120.0 ± 3.0	1.02
137.4	34.5 ± 0.8	158.7	.932	112.0 ± 3.0	1.03
140.1	38.6 ± 0.7	160.2	.941	130.0 ± 2.0	1.03
142.7	41.6 ± 0.7	161.6	.949	146.0 ± 3.0	1.04
145.95	39.9 ± 0.6	163.4	.958	148.0 ± 2.0	1.04

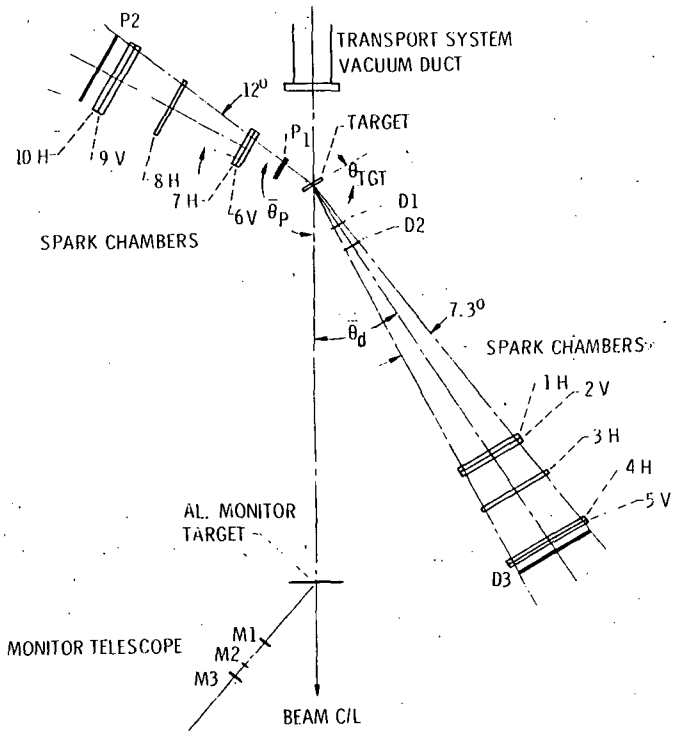

Figure 1. - Experimental arrangement in the proton target area of the NASA synchrocyclotron at the Space Radiation Effects Laboratory.

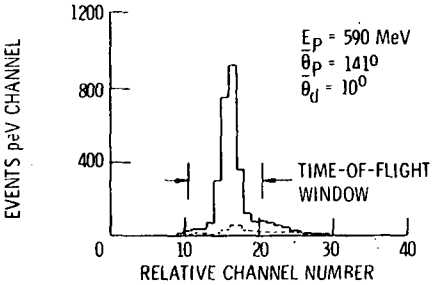

(A) TIME-OF-FLIGHT SPECTRUM AT E_p = 590 MeV, $\bar{\theta}_P$ = 141° AND $\bar{\theta}_d$ = 10°. Solid line for the CD_2 target, dotted line for normalized carbon background.

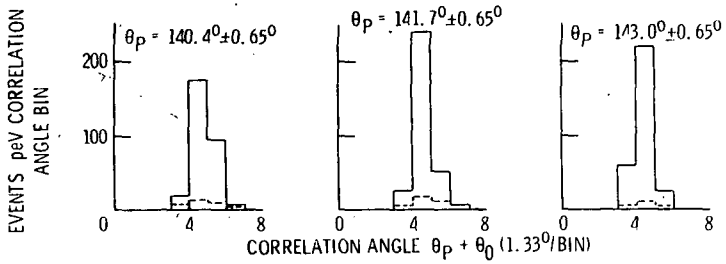

(B) CORRESPONDING SPECTRUM IN CORRELATION ANGLE $\theta_P + \theta_d$ AT θ_P = 140.4°, 141.7°, AND 143.0° FOR EVENTS WITH TIME-OF-FLIGHT WITHIN WINDOW INDICATED IN (A).

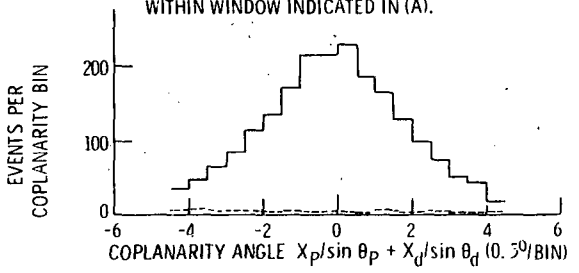

(C) COPLANARITY SPECTRUM FOR EVENTS IN THE TIME-OF-FLIGHT WINDOW INDICATED IN FIGURE (A).

Figure 2

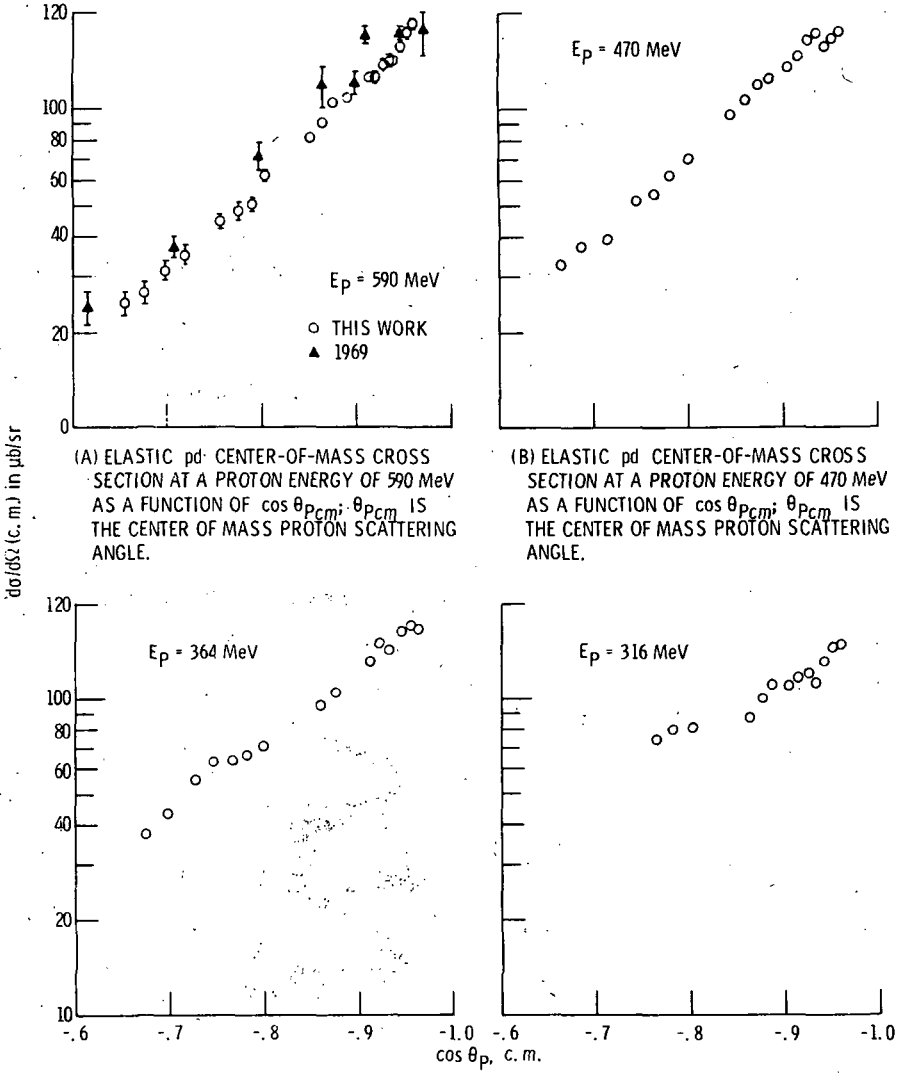

(A) ELASTIC pd CENTER-OF-MASS CROSS SECTION AT A PROTON ENERGY OF 590 MeV AS A FUNCTION OF cos θ_{Pcm}; θ_{Pcm} IS THE CENTER OF MASS PROTON SCATTERING ANGLE.

(B) ELASTIC pd CENTER-OF-MASS CROSS SECTION AT A PROTON ENERGY OF 470 MeV AS A FUNCTION OF cos θ_{Pcm}; θ_{Pcm} IS THE CENTER OF MASS PROTON SCATTERING ANGLE.

(C) ELASTIC pd CENTER-OF-MASS CROSS SECTION AT A PROTON ENERGY OF 365 MeV AS A FUNCTION OF cos θ_{Pcm}; θ_{Pcm} IS THE CENTER OF MASS PROTON SCATTERING ANGLE.

(D) ELASTIC pd CENTER-OF-MASS CROSS SECTION AT A PROTON ENERGY OF 316 MeV AS A FUNCTION OF cos θ_{Pcm}; θ_{Pcm} IS THE CENTER OF MASS PROTON SCATTERING ANGLE.

Figure 3

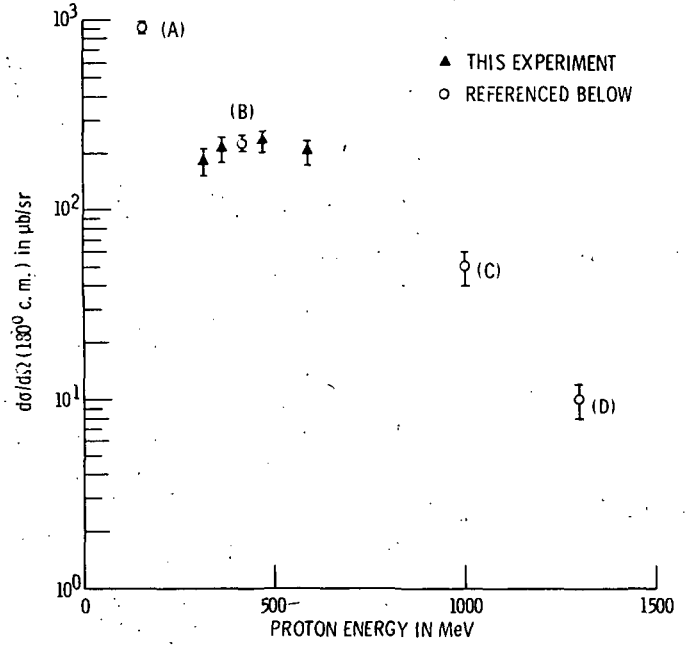

Figure 4. - Extrapolated 180^0 center of mass cross section as a function of proton energy. Points at a, b, c, d were obtained from references 13, 9, 2, 1.